Supporting Information for

Mechanical Properties of Cathode-Electrolyte Interphase Layers in High-Voltage Lithium-Ion Batteries

Xiaotang Shi[1], Andrew Naylor[2], Till Fuchs-Kühn[3], Steffen Schröder[3], Franjo Weber[1], Anja Henss[3], Hans-Jürgen Butt[1], Rüdiger Berger*[1]

[1]Max Planck Institute for Polymer Research, Mainz, 55128, Germany

[2]Department of Chemistry-Ångström Laboratory, Uppsala University, 751 21, Uppsala, Sweden

[3]Institute of Experimental Physics I and Center for Materials Research, Justus Liebig-University Giessen, Heinrich-Buff-Ring 16, 35392 Giessen, Germany

*Corresponding author: berger@mpip-mainz.mpg.de

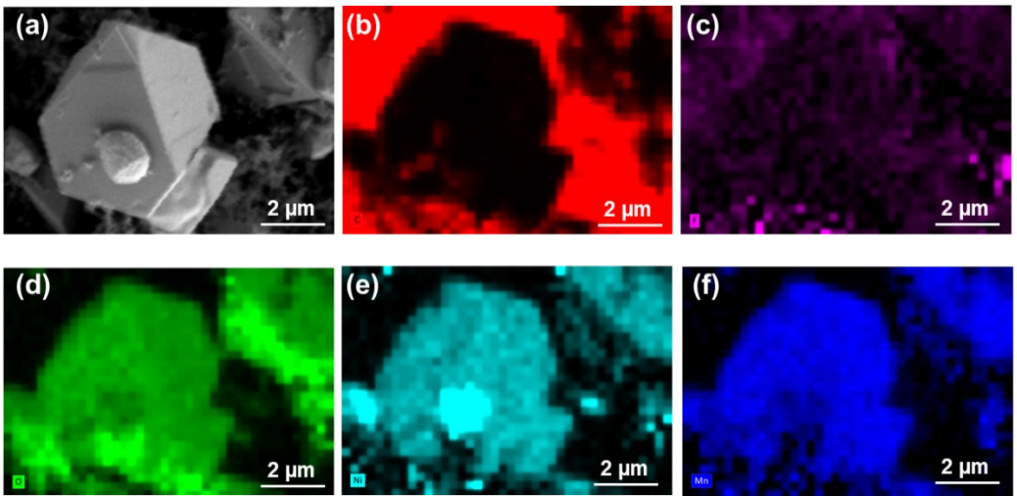

Figure S1. SEM-EDX measurement on pristine LNMO electrode. SEM image of LNMO pristine electrode (a) and EDX element mapping of C (b), F (c), O (d), Ni (e) and Mn (f).

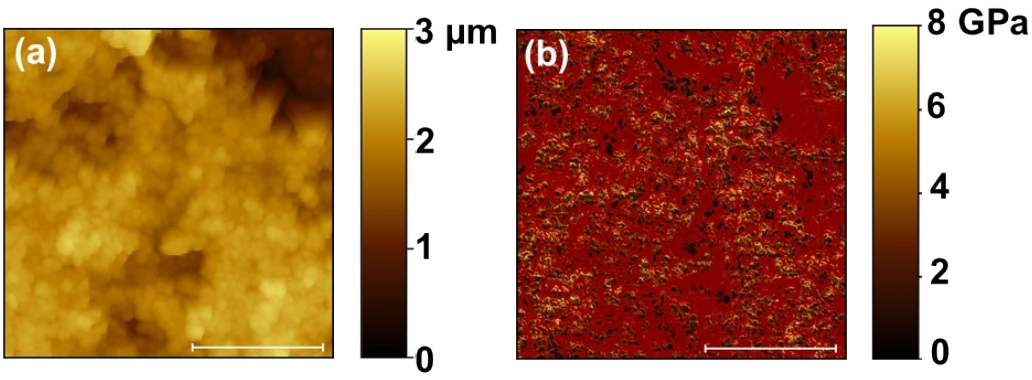

Figure S2. SFM Characterization of the surface of b/c sample. (a) Topography image and (b) calibrated modulus map. Scale bar: 2 µm.

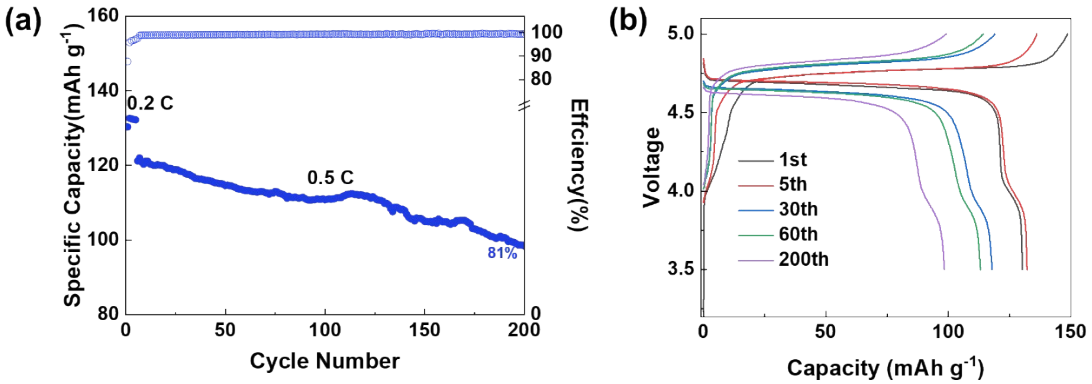

Figure S3. (a) Cycling performance and Coulombic efficiency of LNMO/Li cells and (b) selected charge/discharge curves.

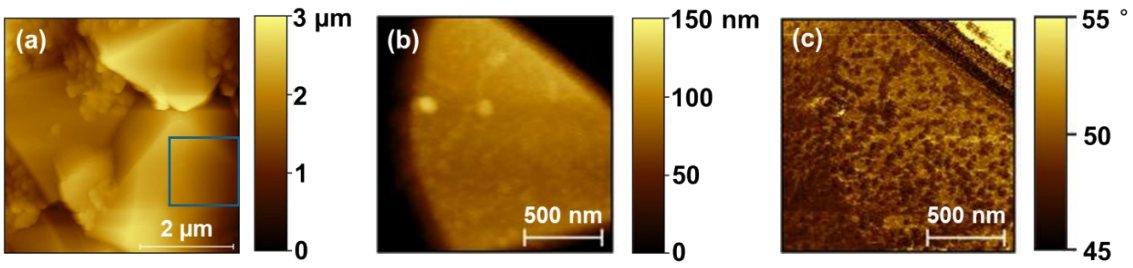

Figure S4. SFM images of LNMO electrode cycled for 5 times. (a) overall topography image, (b) enlarged topography image from the blue-framed position in a), and (c) corresponding phase image.

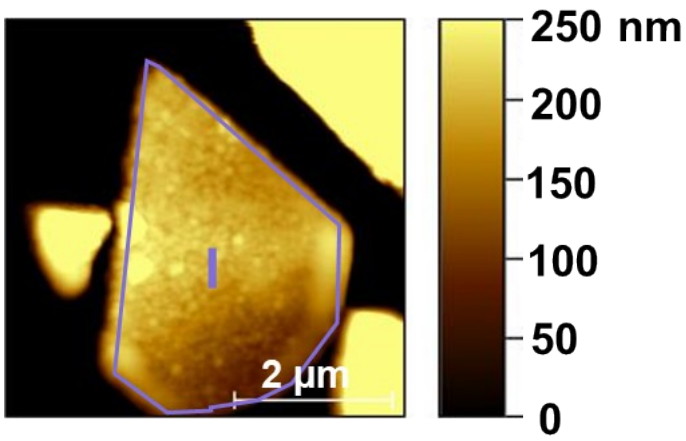

Figure S5. SFM topography image of LNMO electrode cycled for 60 times. The CEI layer appears amorphous with a morphology characterized by rounded particles in region I.

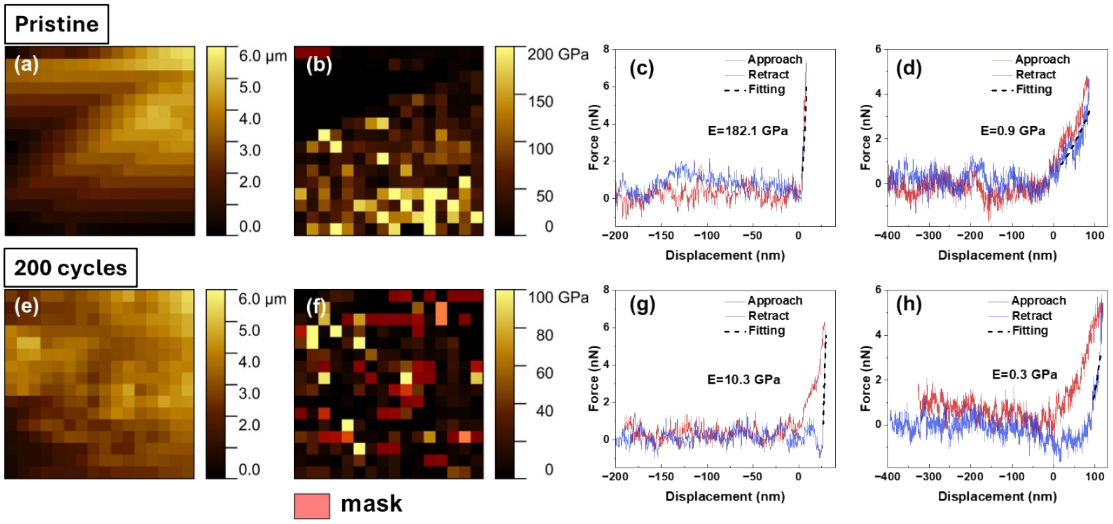

Figure S6. Two nanoindentation measurements on LNMO electrodes: Pristine and after 200 cycles. (a, e) Topography (20 × 20 µm), (b, f) corresponding elastic moduli maps. (c, g) examples of force displacement curves on carbon/binder mixture region. (d, h) examples of force displacement curves on a LNMO.

For the comparison, we performed conventional nanoindentation measurements (Figure S6a-f). The CEI layer has a thickness of ≈ 20 nm. At a load of 6 µN, analyzable loading and unloading curves could be measured. Under these conditions, the indentation depth was approximately 5 nm on the LNMO surface and approximately 100 nm on the carbon/binder (b/c) mixture surface (Figure S6c, d). On the carbon/binder, the indentation depth clearly exceeded the thickness of the CEI layer. On LNMO, we measured a modulus of 182.1 GPa and on the carbon/binder 0.9 GPa.

For Berkovich indenters, a spacing of approximately ten times the maximum indentation depth is required to avoid artifacts in the measured hardness and modulus[1]. Based on this rule, we employed a 16 × 16 indentation grid over a 20 × 20 µm^2 area. At this resolution, LNMO particles and b/c regions are barely distinguishable in the topography maps (Figure S6a, e).

Force-displacement (F-D) curves were recorded at each indentation point, and the elastic moduli were calculated to generate modulus maps. Measurements were classified as invalid when the recorded force–displacement curves showed incomplete loading or unloading segments or lacked a well-defined contact point, preventing reliable mechanical analysis. These invalid measurements were excluded from further analysis by applying a mask to the force map.

A pronounced overall decrease in modulus was observed after 200 electrochemical cycles in a coin cell (Figure S6b, f). Representative single F-D curves were further extracted from the soft b/c regions and hard LNMO regions. For the soft b/c regions (Figure S6c, g), the indentation depth was approximately 100 nm. Therefore, the apparent modulus was strongly influenced by the underlying substrate. For the hard LNMO regions (Figure S6d, h), the loading and unloading curves overlap on the pristine electrode, indicating predominantly elastic deformation. After 200 cycles, the loading curve exhibits two distinct slopes, reflecting the mechanical contrast between the relatively soft CEI layer and the much stiffer LNMO substrate. With increasing indentation depth, a substantial portion of the deformation field penetrates into the underlying metal-oxide substrate, leading to an overestimation of the elastic modulus. We obtained a modulus of approximately 10.3 GPa at an indentation depth of ~30 nm. After 200 cycles, the thickness of the CEI layer is around or higher than 20 nm, resulting in an indentation depth-to-layer thickness ratio close to or exceeding unity. Under such conditions, the

measured modulus reflects the mechanical response of both the CEI layer and the underlying LNMO substrate.

By contrast, the AM-FM measurement on the LNMO surface after 200 cycles showed a modulus of 3.9 ± 0.8 GPa with a maximum indentation depth of approximately 2 nm. Such low depths are well below the estimated CEI thickness and therefore largely free from substrate effects. The lower modulus obtained by the AM-FM method confirms that the nanoindentation results show an overestimated value dominated by substrate contributions.

Moreover, surface roughness and tilt angles of crystallites in conventional nanoindentation introduce uncertainty into the apparent indentation area. In the absence of nanoscale topography information, it is difficult to correct the apparent modulus for these effects using conventional nanoindentation.

In conclusion, both insufficient lateral resolution and excessive indentation depth fundamentally limit the ability of conventional nanoindentation to quantitatively characterize thin CEI layers.

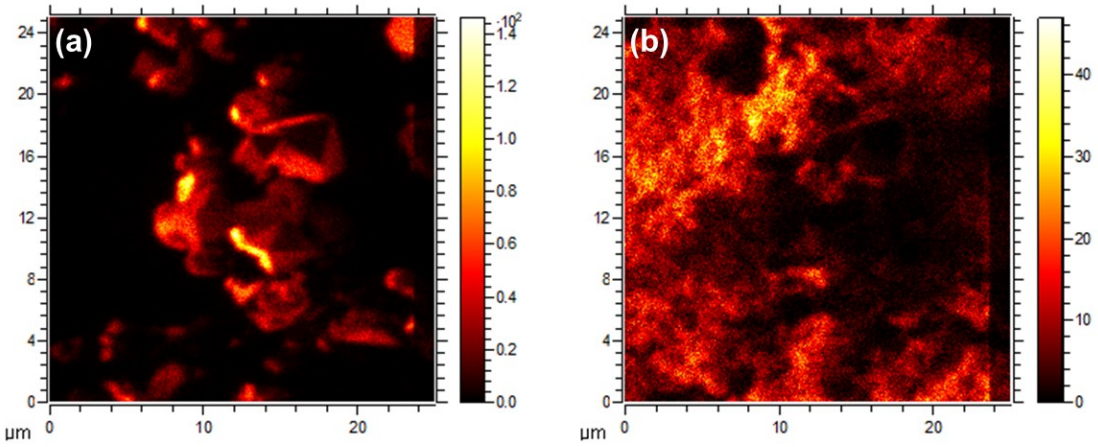

Figure S7. ToF-SIMS images showing the spatial distribution of $^{NiO_2^-}$- and $^{C_2^-}$ fragments on pristine LNMO electrodes.

ToF-SIMS mapping of fragment ion distributions on the pristine electrode reveals $^{NiO_2^-}$-fragments originating from $LiNi_{0.5}Mn_{1.5}O_4$ (LNMO) while $^{C_2^-}$-fragments are associated with the conductive carbon regions (Figure S7). This contrast enables a reliable spatial distinction between LNMO particle regions and binder/carbon (b/c) domains. Furthermore, this approach allows for the analysis of the converged b/c region, which exhibits similar CEI-like mechanical characteristics.

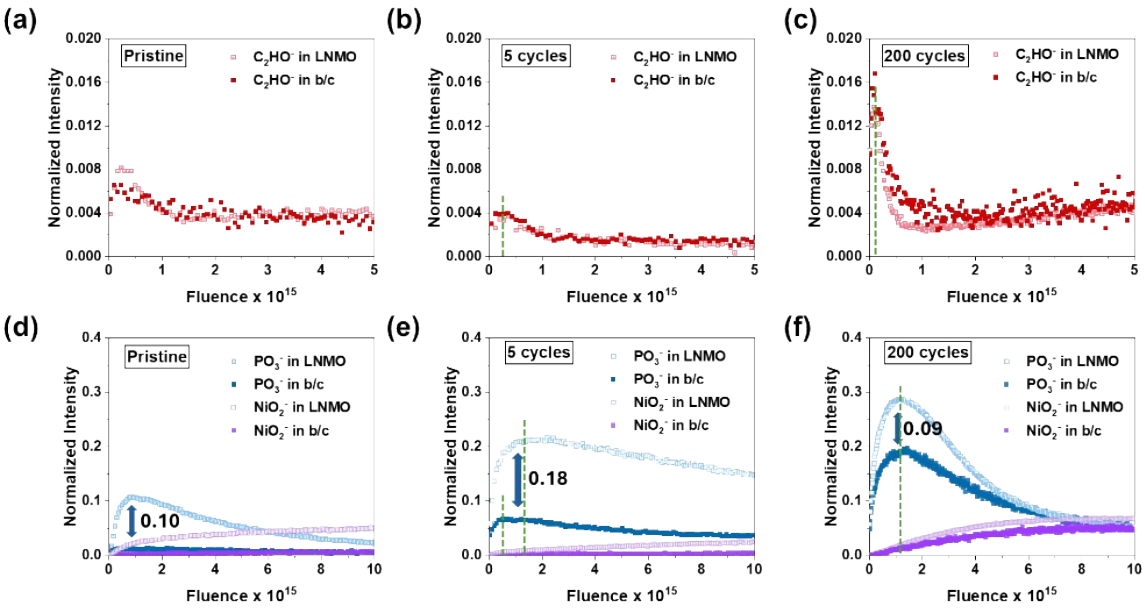

Figure S8. ToF-SIMS depth profiles of LNMO showing signal intensities evolution of C_2HO^- (a-c) and PO_3^-, NiO_2^- (d-f) for electrodes before cycling and after 5 and 200 cycles, respectively (normalized to total ion counts).

The depth profiles of different ion fragments on both LNMO particles and b/c regions (Figure S8) are plotted as a function of sputter ion fluence. The presence of C_2HO^--fragments is attributed to electrolyte decomposition products[2]. The profile shows a small enrichment of C_2HO^- at the surface of the pristine electrodes attributed to adsorbed adventitious carbon and residual organic species from electrode processing, rather than electrochemically formed interphase layers (Figure S8a). After 5 and 200 times, the surface of the LNMO electrode becomes covered by a thin interphase layer. The normalized intensity profiles of C_2HO^--fragments are similar in both LNMO and b/c regions (Figure S8b, c) of the cycled electrodes.

PO_3^--fragments originate from the decomposition of the conducting salt in the electrolyte (Li_3PO_4)[3]. A surface enrichment of PO_3^- is also observed in the LNMO regions of the pristine electrode (Figure S8d), which can be attributed to the very high ionization probability of these fragments. In addition, trace amounts of phosphorous species are present even in battery grade materials, and samples were stored under identical atmospheric conditions for extended periods prior to measurement. After 5 cycles, the normalized intensity difference of PO_3^- between the LNMO and b/c regions is around 0.18 (Figure S8e). After 200 cycles, this difference decreases to 0.09 (Figure S8f). Meanwhile, NiO_2^--fragments are associated with the active material and originate either from the bulk LNMO electrode or from dissolved Ni species. An increased NiO_2^- signal can be detected in the b/c region after 200 cycles (Figure S8f), likely due to the dissolution and redeposition of transition-metal species under high-voltage and prolonged cycling conditions.

Based on the ToF-SIMS analysis, after 200 cycles, the reduced intensity difference of PO_3^- corresponds to a reduced modulus contrast between the CEI and non-CEI layers, which is from 3.2 ± 1.1 GPa vs. 1.6 ± 0.3 GPa to 3.9 ± 0.8 GPa vs. 3.6 ± 0.4 GPa[4]. The increased modulus of the non-CEI layer suggests that the b/c region becomes fully covered by electrolyte decomposition products, forming an interphase layer with a composition increasingly similar to the CEI on LNMO particles. Comparison

of the fluence positions of each peak (green curve in Figure S8c, f) after 200 cycles reveals that organic species are enriched in the outer interphase region, whereas inorganic species dominate the inner region[5]. This layered interphase structure is also observed in the b/c region after long-term cycling (green curve in Figure S8b, e). In contrast, after only 5 cycles, the non-CEI layer does not exhibit a distinct layered structure as both C_2HO^- and inorganic PO_3^- signals in the b/c region show similar depth evolution.

Overall, the ToF-SIMS results show convergence of C_2HO^-, PO_3^- and NiO_2^--fragments intensities between LNMO and b/c regions, suggesting that the interphase formed on the b/c region progressively evolves toward a CEI-like chemical composition during long-term cycling. This chemical convergence also directly corroborates the SFM results and explains the observed modulus convergence between the inactive region and the CEI.

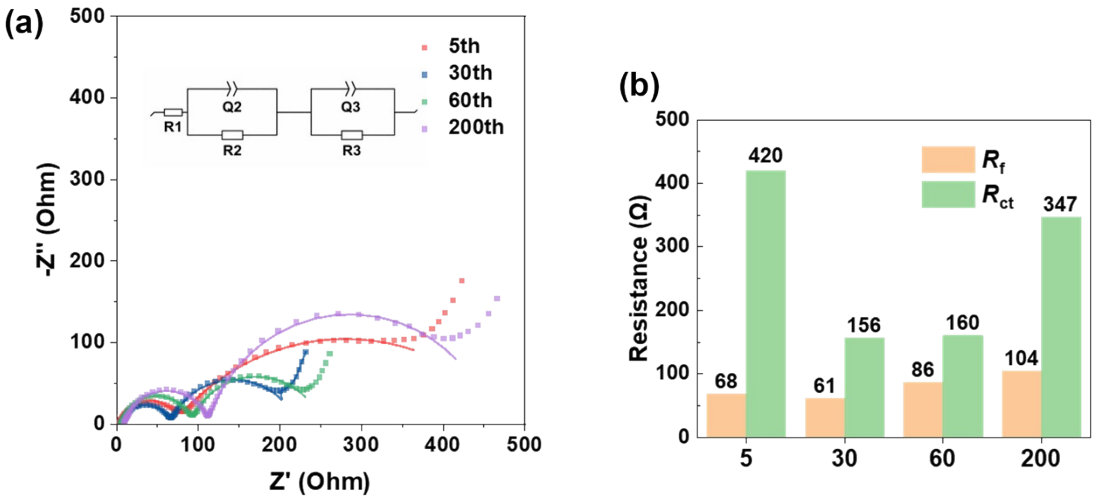

Figure S9. (a) Nyquist plots and its fitting results of the LNMO/Li cells after 5, 30, 60 and 200 cycles and (b) its corresponding R_f and R_{ct} extracted from fitting results.

In composite electrodes containing both electrochemically active and inactive phases, the impedance parameters extracted from EIS represent the equivalent response of the entire electrode rather than isolated contributions from individual components. The formation of interphase layers on inactive regions can modify ion-transport pathways, reduce the effective electrochemically active area, and alter local reaction environments, thereby contributing to the observed increases in R_f and R_{ct}. Furthermore, the interphase evolution is also reflected in the increased voltage hysteresis observed in the Q-V curves (Figure S3b). The increased polarization correlates well with the degradation of ion-transport and charge-transfer kinetics inferred from the EIS results. Therefore, the concurrent evolution of impedance and voltage hysteresis is interpreted as a coupled electrochemical consequence of interphase formation throughout the composite electrode, rather than being solely attributable to the interphase on either the active or inactive material alone.

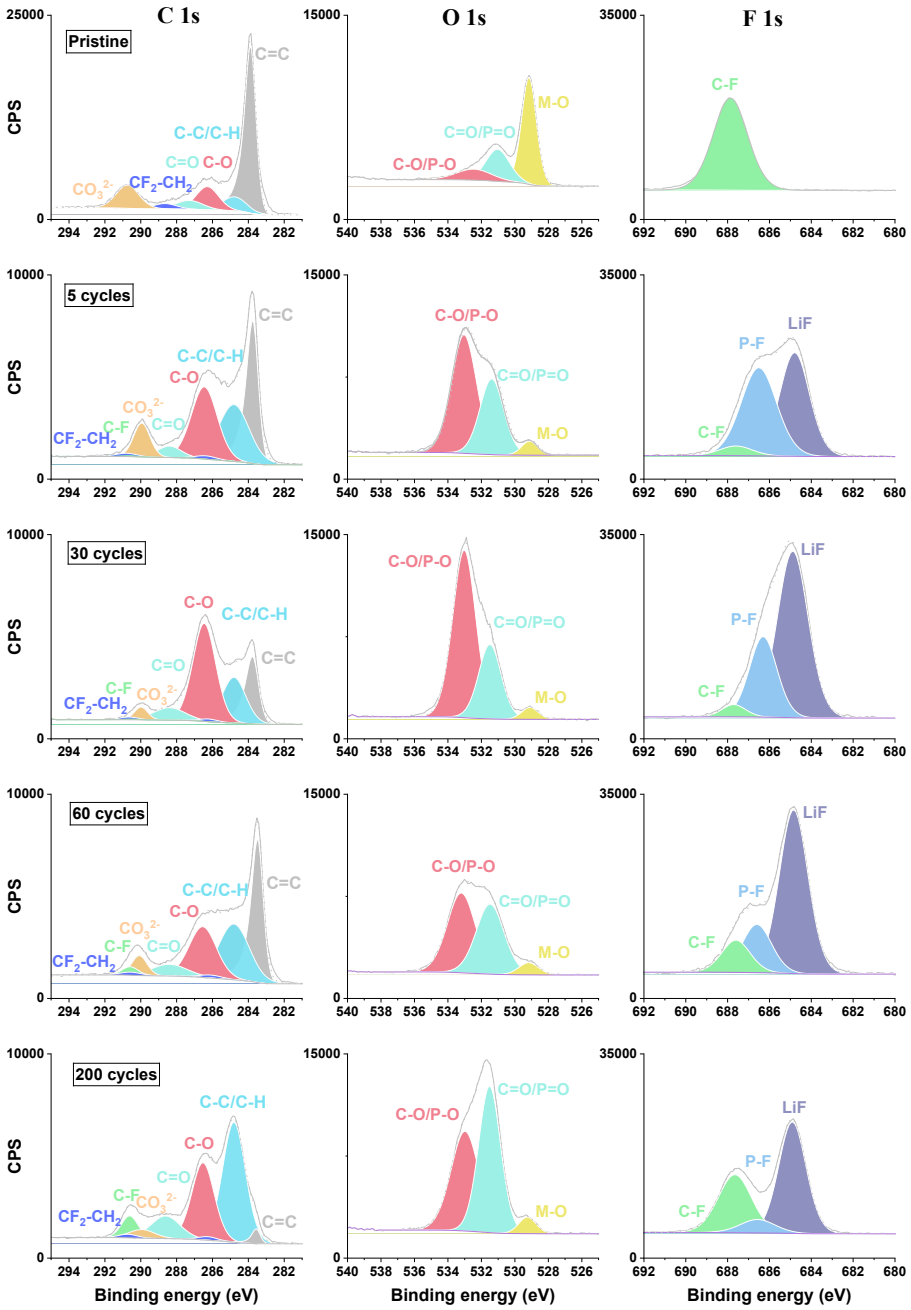

Figure S10. XPS C 1s, O 1s and F 1s spectra of the LNMO electrode before and after 5, 30, 60, 200 cycles.

Table S1. XPS Peak Binding Energy and Assignments

Spectra	Binding energy (eV)	Assignment
C 1s	283.5-283.8	C=C
	284.8	C-C
	286.1-286.4 290.6-290.8	CH_2 - CF_2
	286.5	C-O
	288.4-288.6	C=O
	290	CO^{2-}_3
	290.5-290.6	C-F
O 1s	529.0-529.3	M-O
	531.0-531.4	C=O, P=O
	532.4-533.1	C-O, P-O
F 1s	684.8-684.9	LiF
	686.3-686.6	P-F
	687.6-687.9	C-F

References

1. P. Sudharshan Phani and W. C. Oliver, *Materials & Design*, 2019, **164,** 107563.
2. W. Li, A. Dolocan, P. Oh, H. Celio, S. Park, J. Cho and A. Manthiram, *Nat Commun*, 2017, **8**, 14589.
3. H. Ren, G. Zheng, Y. Li, S. Chen, X. Wang, M. Zhang, W. Zhao, H. Yi, W. Huang, J. Fang, T. Liu, L. Yang, M. Liu, Q. Zhao and F. Pan, *Energy & Environmental Science*, 2024, **17**, 7944-7957.
4. H. Ren, J. Hu, H. Ji, Y. Huang, W. Zhao, W. Huang, X. Wang, H. Yi, Y. Song, J. Liu, T. Liu, M. Liu, Q. Zhao and F. Pan, *Adv Mater*, 2024, **36**, e2408875.
5. C. Weng, M. Qiu, B. Wang, J. Yang, W. Mai, L. Pan, S. Huang and J. Li, *Angew Chem Int Ed Engl*, 2025, **64**, e202419539.